



This is a repository copy of *Oxygen stoichiometry, chemical expansion or contraction and electrical properties of rutile, TiO<sub>2</sub>+/-delta ceramics*.

White Rose Research Online URL for this paper:  
<http://eprints.whiterose.ac.uk/132776/>

Version: Accepted Version

---

**Article:**

Dang, Y. and West, A. [orcid.org/0000-0002-5492-2102](https://orcid.org/0000-0002-5492-2102) (2018) Oxygen stoichiometry, chemical expansion or contraction and electrical properties of rutile, TiO<sub>2</sub>+/-delta ceramics. *Journal of the American Ceramic Society*, 102 (1). pp. 251-259. ISSN 0002-7820

<https://doi.org/10.1111/jace.15889>

---

**Reuse**

Items deposited in White Rose Research Online are protected by copyright, with all rights reserved unless indicated otherwise. They may be downloaded and/or printed for private study, or other acts as permitted by national copyright laws. The publisher or other rights holders may allow further reproduction and re-use of the full text version. This is indicated by the licence information on the White Rose Research Online record for the item.

**Takedown**

If you consider content in White Rose Research Online to be in breach of UK law, please notify us by emailing [eprints@whiterose.ac.uk](mailto:eprints@whiterose.ac.uk) including the URL of the record and the reason for the withdrawal request.



[eprints@whiterose.ac.uk](mailto:eprints@whiterose.ac.uk)  
<https://eprints.whiterose.ac.uk/>

# Oxygen stoichiometry, chemical expansion or contraction and electrical properties of rutile, $\text{TiO}_{2\pm\delta}$ ceramics

Yun Dang and Anthony R. West<sup>1</sup>

Department of Materials Science and Engineering, University of  
Sheffield, S1 3JD, Sheffield, UK

## ABSTRACT

*Rutile,  $\text{TiO}_2$  is increasingly oxygen-deficient on heating in air above  $\sim 700$  °C. The weight loss is generally too small for accurate measurement, but the electrical properties of quenched samples provide a sensitive qualitative indicator of oxygen content since their conductivity can vary by many orders of magnitude. The oxygen lost at high temperature is fully recovered if samples are cooled slowly. With rapid quenching, by dropping samples into liquid  $\text{N}_2$ , the oxygen stoichiometry at high temperature is preserved to ambient and the resulting materials are kinetically stable but thermodynamically metastable. The lattice parameters of quenched samples showed an unusual dependence on quench temperature and, by implication, on oxygen stoichiometry. Lattice parameters increased with a small oxygen loss,  $\delta$ ; chemical expansion of the lattice occurred and is attributed to reduction in average Ti oxidation state and increase in Ti-O bond lengths. At higher  $\delta$ , lattice parameters started to decrease giving a chemical contraction effect attributed to partial collapse*

---

<sup>1</sup> Correspondence email: a.r.west@sheffield.ac.uk

*of columns of edge-sharing  $TiO_6$  octahedra in the rutile structure and elimination of oxygen vacancies by crystallographic shear plane formation.*

*Oxygen-deficient samples quenched from above 700 °C were n-type, as were samples annealed and measured at 650 and 700 °C. Samples measured at 450-500 °C were p-type and believed to be slightly oxygen-rich; it is suggested that holes located on oxide ions at or near the sample surface arose from redox electron transfer between under-bonded surface oxide ions and adsorbed  $O_2$  molecules. Samples annealed between 550 and 600 °C showed cross-over between n- and p-type behavior.*

## **1. Introduction**

$TiO_2$  is an important functional material with a diverse range of applications in the form of ceramics, films or nanoparticles. For instance:  $TiO_2$  has good brightness and can block UV light, which gives it applications as a component of white paints;  $TiO_2$  is a promising and critical photoanode of Dye-Sensitized Solar Cells since it has unique photovoltaic and photochemical properties; it is widely employed as a photo-catalyst and was the key active component of the first memristor.<sup>1-4</sup>

In its pure, oxygen-stoichiometric form,  $TiO_2$  is a white insulating solid with a bandgap of 3.2 eV. On heating, it increasingly loses oxygen above ~700 °C in air<sup>5</sup>. The electrons that are released enter the Ti 3d conduction band, as shown by a large increase in electronic conductivity, either by direct measurement at high temperature or by measuring, at lower temperatures, the conductivity of quenched samples. For instance, ceramics quenched from 1300 °C are good n-type semiconductors with typical conductivity  $10^{-1} \text{ Scm}^{-1}$  and activation energy 0.01 eV over a wide temperature range down to 20 K. More extensive oxygen loss occurs on heating in a reducing atmosphere giving rise to so-called black rutile.<sup>6</sup>

Crystallographic shear (CS) structures in non-stoichiometric rutile were first found by the Magnéli group.<sup>7</sup> They reported that certain transition metal oxides, including TiO<sub>2</sub>, WO<sub>3</sub> and MoO<sub>3</sub>, formed homologous series of CS structures, rather than continuous solid solutions, on reduction. Their discovery had a strong impact on understanding the crystal chemistry and defect structures of non-stoichiometric compounds. Heavily-reduced rutile forms a homologous series of CS phases of general formula Ti<sub>n</sub>O<sub>2n-1</sub>. The oxygen vacancies that form on initial reduction are subsequently eliminated by a partial collapse of the structure to form CS planes. A study of lightly-reduced rutile by transmission electron microscopy, TEM, showed the presence of random CS planes in a sample quenched from 1050 °C and annealed at lower temperature.<sup>8</sup>

The present work arose from a study into the effect of acceptor dopants on the electrical properties of rutile. In particular, the doped materials commonly showed *p*-type electrical conductivity and it was of interest to determine the conditions, if any, under which undoped rutile may also show *p*-type behavior. As part of this study, the lattice parameters of rutile quenched from various temperatures were recorded in the anticipation that chemical expansion effects associated with oxygen loss may be observed. The surprising result was obtained that indeed, chemical expansion does occur initially but is replaced by chemical contraction at higher oxygen loss. This anomalous variation in lattice parameters is attributed to a combination of two competing effects: oxygen loss and CS plane formation.

## 2. Experimental

TiO<sub>2</sub> (rutile, <5 μm particle size, ≥99.9% purity, Aldrich, UK; [analytical data are given in Table S1.](#)) powders were used as received. Initially, samples were heated at 900 °C for 6 h to remove any volatile material and convert any anatase particles to rutile. Small quantities were then heated in Pt envelopes in a vertical tube quench furnace

in an atmosphere of either air or N<sub>2</sub> for 1 h before quenching into liquid N<sub>2</sub>. Cooling rates are estimated as ~500 °C sec<sup>-1</sup>. For X-ray diffraction, XRD, a STOE-STADI Cu PSD diffractometer with Si internal standard was used. XRD data are shown in Fig S1 for samples that had been heated at 1300 °C and either cooled slowly or quenched into liquid N<sub>2</sub>. These therefore represent the extremes of oxygen content that could be expected in the samples studied here. Both patterns [also](#) contain peaks associated with Si internal standard; all remaining peaks were indexed on the tetragonal rutile unit cell [and lattice parameters obtained by least squares refinement](#).

For electrical property measurements, pellets [\(8 mm diameter and 1-2 mm thick\)](#) were prepared by either uniaxial pressing or cold isostatic pressing and sintered at 1250 °C for 8 h to give a final density of ~92%. Electrodes were fabricated on opposite pellet faces using Pt paste (C3657 conductor paste, Heraeus Deutschland GmbH & Co.) which was decomposed and hardened by heating at 900 °C for 2 h. The pellets with electrodes attached were placed in an in-house conductivity jig inside a horizontal tube furnace; impedance measurements were made in either air, N<sub>2</sub> or O<sub>2</sub> using a combination of Agilent 4980A, Modulelab XM Solartron and Solartron SI 1260 instrumentation. A nominal *ac* voltage of 100 mV was used. [Impedance data were corrected for overall sample geometry and resistance values are therefore reported with unit of ohms cm.](#)

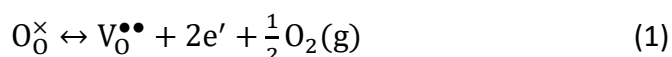
Most of the impedance results reported here are for the same sample that was equilibrated sequentially in O<sub>2</sub>, air and N<sub>2</sub> for 3 h at each temperature prior to impedance measurements. Measurements commenced at 700 °C and were repeated on stepwise cooling at 50 °C intervals over the range 700-450 °C. Separate tests showed that the observed changes in conductivity on changing pO<sub>2</sub> were essentially reversible and that a steady state was reached after 1-2 h.

### 3. Results and Discussion

### 3.1 Lattice parameters

Lattice parameter and unit cell volume data for rutile powders heated at different temperatures in either air or N<sub>2</sub> and quenched into liquid N<sub>2</sub> are shown in Figure 1. Data are also shown for a sample that was slow-cooled from 1250 °C in air. All the XRD patterns that were used to calculate these lattice parameters showed no discernable differences from that of a standard rutile pattern, apart from small variations in peak positions. As examples, two patterns that represent the extremes of oxygen content  $\delta$ , for samples that were either slow-cooled in air or quenched into liquid N<sub>2</sub>, are shown in Figure S1. Two types of behavior can be distinguished, for samples quenched from 700-1000 °C and for samples quenched from 1200-1300 °C.

On quenching from 700-1000 °C, the parameters increased rapidly with quench temperature, Figure 1. All the data were recorded at room temperature and therefore, should not show effects associated with standard thermal expansion. The increases in lattice parameters are instead attributed to chemical expansion associated with loss of oxygen with increasing quench temperature, eq'n (1), to give non-stoichiometric rutile, with oxygen vacancies, of general formula TiO<sub>2- $\delta$</sub> .



A consequence of oxygen loss is the release of electrons which effectively reduce some Ti<sup>4+</sup> to Ti<sup>3+</sup>. A combination of the larger radius of Ti<sup>3+</sup>, a weaker Ti-O bond strength and an increase in average Ti-O bond length, similar to that reported with other oxides<sup>9,10</sup>, leads to chemical expansion.

On quenching from above 1000 °C, lattice parameters did not increase any further but instead, reached a maximum and then decreased, especially for samples annealed in N<sub>2</sub>. The oxygen loss represented by eq'n (1) is expected to continue with increasing temperature, especially on reducing the oxygen partial pressure in the surrounding atmosphere and displacing the equilibria to the right. An additional

factor must therefore influence the lattice parameters and cell volume of samples with larger  $\delta$  values. We did not obtain lattice parameter data for samples annealed at high temperature in oxygen, but it is anticipated that these would lose less oxygen at high temperatures and the decrease in lattice parameters would therefore be less than that of samples annealed in air.

It is well-established that CS structures form in materials such as acceptor-doped  $\text{TiO}_2$ ,  $\text{Nb}_2\text{O}_5$ ,  $\text{MoO}_3$  and  $\text{WO}_3$  as a means of eliminating oxygen vacancies. This leads to a partial collapse of the crystal structures to form CS planes. We consider it highly likely that similar CS planes form in oxygen-deficient rutile as the degree of oxygen-deficiency increases; [the observed decrease in lattice parameters and cell volume is attributed to transformation of edge-sharing octahedra to face-sharing octahedra in the CS planes](#). At this stage, we have no direct evidence ourselves for the CS planes, nor whether they are random planar defects in the rutile lattice or form ordered Magneli structures. There is, however, clear evidence in the literature<sup>8</sup> of CS plane formation in samples of composition  $\text{TiO}_{1.9970}$  which were quenched from 1050 °C and subsequently annealed at lower temperature. From the data shown in Figure 1, it appears that CS planes start to form in air at temperatures as low as 1100 °C where the **lattice expansion** due to oxygen loss begins to be offset by the **lattice contraction** associated with CS plane formation.

### ***3.2 Electrical properties***

It is well-established that rutile loses an increasing amount of oxygen with increasing temperature above 700 °C<sup>5,11-21</sup>. The resulting materials are *n*-type semiconductors as shown by first, an increase in conductivity with decreasing  $p\text{O}_2$  in the atmosphere surrounding the sample during impedance measurements, eq'n (1) and second, by a decrease in conductivity on application of a small *dc* bias voltage during the impedance measurements.<sup>11</sup> Although the amount of oxygen loss was barely

detectable by thermogravimetry, dramatic changes in conductivity were observed and for instance, rutile quenched from 1300 °C had stoichiometry  $\delta=0.001$  in  $\text{TiO}_{2-\delta}$ , and a conductivity of  $\sim 10^{-1} \text{ Scm}^{-1}$  for temperatures down to 20 K<sup>5</sup>, which is many orders of magnitude higher than that of oxygen-stoichiometric  $\text{TiO}_2$ .

In this paper, we focus on rutile ceramics that were annealed and measured between 700 and 450 °C. At 700 °C, the samples were still weakly *n*-type but changed to *p*-type at lower annealing temperatures. Impedance data recorded at 700 °C and measured in atmospheres of  $\text{O}_2$ , air and  $\text{N}_2$  are shown in Figure 2. In order to achieve kinetic equilibration of the sample prior to measurements, the sample was loaded into the impedance jig and left at 700 °C for 3 h. By kinetic equilibration, we mean that the sample surface is in equilibrium with oxygen adsorption/ionization/dissociation processes that take place at the sample surface; it is highly unlikely that full equilibration with the sample interior is achieved at these temperatures and times.

The impedance data, Figure 2, indicate the presence of two distorted arcs in the complex plane plots (A) which are attributed to bulk and grain boundary resistances,  $R_1$  and  $R_2$  respectively. In all cases, at 700 °C the resistances of both components increased with increasing  $p\text{O}_2$ . Since the effect of increasing  $p\text{O}_2$  is to drive the equilibrium shown in equation (1) from right to left, electrons are removed from the sample and the observed increase in resistance shows that the samples are *n*-type. Since  $R_1$  and  $R_2$  refer to sample bulk resistances, this observation indicates that changes to the electronic structure in the sample interior are controlled by defect equilibria at the sample surface.

The impedance results also indicate that, although conduction is essentially *n*-type at 700 °C, there may also be a small amount of oxide ion conduction since the  $\log C'/\log f$  data (B) show a low-frequency capacitance as high as  $5 \times 10^{-7} \text{ Fcm}^{-1}$  for the sample measured in  $\text{N}_2$ . The corresponding capacitance data in air and  $\text{O}_2$  are smaller. These high capacitance values are attributed to the presence and mobility of oxygen



vacancies in the lightly-reduced sample which are blocked at the electrodes. The smaller capacitance values in air and O<sub>2</sub> may indicate that the concentration of mobile oxygen vacancies is smaller, consistent with equation (1) and the expectation of a reduced oxygen vacancy content, especially at the surface, of samples heated in air and O<sub>2</sub>. Similar results and conclusions were obtained for the sample annealed and measured at 650 °C.

Using a similar procedure, impedance data were obtained for the sample annealed and measured at 450 and 500 °C; the results at 500 °C are shown in Figure 3. However, resistances R<sub>1</sub> and R<sub>2</sub> showed the opposite dependence on pO<sub>2</sub> and were greatest in N<sub>2</sub> but smallest in O<sub>2</sub>, consistent with *p*-type behavior.

Impedance data at 550 °C and 600 °C showed a cross-over between *n*-type and *p*-type behavior. At 600 °C, Figure 4(A), data in N<sub>2</sub> and air show clearly an *n*-type response but a small switch to *p*-type when measured in O<sub>2</sub>. At 550 °C, Figure 4(B), the sample is still *n*-type on comparing the data measured in N<sub>2</sub> and air, but is more clearly *p*-type in O<sub>2</sub>.

The various conductivity responses for temperatures in the range 400-700 °C are interpreted using the schematic variation of conductivity with pO<sub>2</sub> shown in Figure 5 and as shown experimentally by isothermal measurements of conductivity vs pO<sub>2</sub> at higher temperatures<sup>16-21</sup>. Diagram (A) shows *n*- and *p*- type regions at low and high pO<sub>2</sub>, respectively. In the *n*-type region, the variation of conductivity with pO<sub>2</sub> may have an ideal slope of either -1/6 or -1/4 on logarithmic scales and a slope of +1/4 for *p*-type behavior<sup>16-21</sup>. In the absence of any oxide ion conduction, the electronic conduction changes from *n*-type to *p*-type in a cross-over region. Although we do not have data over a wide pO<sub>2</sub> range and have not studied the quantitative variation of conductivity with pO<sub>2</sub>, measurements in O<sub>2</sub>, air and N<sub>2</sub>, with pO<sub>2</sub> values of 1, 0.21 and approximately 0.001 respectively, nevertheless enable a qualitative interpretation of the experimental conductivity data based on the schematic changes shown in (A). Thus, at 650 and 700 °C, samples are clearly *n*-type in all three

atmospheres, N<sub>2</sub>, air and O<sub>2</sub>, (B). Likewise, at 450 and 500 °C, samples are *p*-type in all three atmospheres, (C). At 550 °C and 600 °C, samples are in, or near, the cross-over region (not shown); they appear to be mainly *n*-type in N<sub>2</sub> and *p*-type in O<sub>2</sub>, but their precise behavior in air is uncertain.

Capacitance data at 700 °C, Figure 2(B), show high values at low frequencies which are indicative of a certain amount of oxide ion conduction, especially close to sample surfaces and therefore, a small domain of electrolytic, or partial electrolytic behavior may be expected at intermediate pO<sub>2</sub> values, as shown in Figure 5(A), lower diagram. In the present case, we do not believe that there is a wide electrolytic domain of exclusively oxide ion conduction but instead, a narrow domain of pO<sub>2</sub> values over which mixed electronic conduction and a small amount of oxide ion conduction occurs. These results are for samples that after annealing for 3 h at each temperature, were presumed to be in equilibrium concerning oxygen gas-solid oxide interactions at sample surfaces. Nevertheless, the electron distribution and concentration in the sample interior is able to respond to the changes in surface equilibria, even though the ionic defect structure of sample interiors is effectively frozen-in. Specifically, electrons may be withdrawn from/added to sample interiors in response to changes at the surface.

The observed *p-n* transition is qualitatively similar to that based on defect equilibria calculations and detailed conductivity measurements as a function of pO<sub>2</sub> with transition temperatures reported variously of 1273 K at 10<sup>4</sup> Pa, 1073 K at 10<sup>2</sup> Pa<sup>20</sup> and an extrapolated temperature of 515 K at 10<sup>-10</sup> Pa O<sub>2</sub>. Differences in the *p-n* cross-over temperature reported here and those in the literature<sup>20</sup> may be associated with the difficulties in obtaining true thermodynamic equilibrium at lower temperatures, especially equilibria involving immobile defects such as Ti vacancies for which times of about 1000 h are required to establish equilibrium at 1323 K in comparison with 10-20 minutes for equilibration of Ti interstitials and oxygen vacancies<sup>20</sup>.

We now consider the possible origins of the *n*- and *p*-type behavior. For the *n*-type materials quenched from 700 °C and above,<sup>5</sup> the reported activation energy varied enormously between 0.67 and 0.01 eV as the degree of oxygen loss and hence the conductivity, increased. An Arrhenius plot showing the conductivity of samples quenched from temperatures in the range 700 to 1400 °C is reproduced in Figure 6.<sup>5</sup> These oxygen-deficient quenched samples were all kinetically stable and did not undergo re-oxidation during conductivity measurements over the temperature ranges shown. In order to account for the large variation in activation energy with  $\delta$ , it appears that electrons associated with oxygen loss must occupy discrete inter-gap states, as shown schematically in Figure 7(A). With increasing  $\delta$ , discrete levels higher in the bandgap are increasingly occupied and the activation energy for conduction, which represents promotion of electrons from inter-gap states to the conduction band, decreases. The dark color of *n*-type samples quenched from high temperature is attributed to absorption of visible light and promotion of electrons from the occupied inter-gap states. The absence of occupied inter-gap states accounts for the white color of slow-cooled samples.

The effect of  $pO_2$  on *n*-type conductivity is readily explained using eq'n (1) since only one variable, the number of pre-existing electronic charge carriers is involved. With increasing  $pO_2$ , electrons are withdrawn from the sample, trapped by the formation of reduced oxygen species at the surface and therefore, the conductivity decreases. This should occur equally at all surfaces on changing  $pO_2$  and lead to a slight charge imbalance between sample surface and interior<sup>22</sup>. With decreasing  $pO_2$ , the opposite effect occurs: reduced oxygen species are desorbed from the sample surface, the released electrons increase the charge carrier concentration in the sample interior and the conductivity increases.

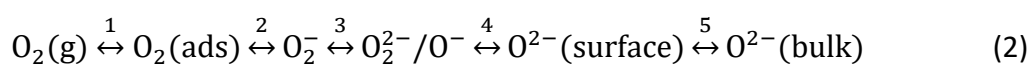
A similar explanation applies, in principle, to the effect of  $pO_2$  on *p*-type conductivity, but the reactions involved are more complex since, although the surface equilibria in eq'n (1) involve changes in *electron* concentration, the resulting

conductivity **variation** involves changes in *hole* concentration. Holes must therefore be created / annihilated in response to the changes in  $pO_2$  implied by eq'n (1). It is easy to see that, with decreasing  $pO_2$  in the *p*-type region, electrons are liberated which annihilate holes and reduce the conductivity. But, for the opposite reaction to occur with increasing  $pO_2$ , it is necessary to have a spontaneous or facile mechanism of hole creation together with trapping of the liberated electrons.

We now consider the location of holes responsible for the *p*-type conductivity in samples annealed at lower temperatures. We note that although *p*-type conductivity is widely observed in undoped materials, the origin and location of the holes in bulk materials is rarely discussed.

Hole creation requires the presence of a redox-active species that can readily ionize. In principle, there are three possible locations of holes in rutile: Ti, impurities or O. First, since Ti is in its maximum possible valence state, +4, it cannot be oxidized further and be the source and location of holes. Second, unwanted impurities such as Fe could be the location of holes, but high purity, reagent grade  $TiO_2$  was used for the experiments, [Table S1](#), and it is regarded as unlikely that such impurities are responsible. Third, oxide ions are regarded as the likely source and location of holes **since** similar observations were made, and conclusions reached, to explain *p*-type conductivity in numerous  $BaTiO_3$ -related materials.<sup>27-29</sup>

Oxygen ions have the possibility to adopt oxidation states of -1 in either the peroxide ion,  $O_2^{2-}$  or the  $O^-$  ion, as well as oxidation state -1/2 in the superoxide ion,  $O_2^-$ . Surface science studies show the presence of ions such as superoxide and peroxide at the surfaces of many materials.<sup>20, 23-26</sup> Although we have no direct data for the present material, the following equilibria are likely to be present at rutile surfaces:



The various equilibria may be displaced to the right, by either increasing  $pO_2$  or application of a positive bias, both of which involve (1) removal of electrons from the sample and (2) increase in concentration of reduced oxygen species at the sample surface.

In order to account for the facile formation of  $O^-$  ions, ionization of  $O^{2-}$  ions is required, which corresponds to the reverse of step 4, eq'n (2). The key consideration in this is that oxide ions,  $O^{2-}$ , located at sample surfaces and interfaces may be coordinatively unsaturated and under-bonded if their immediate coordination environment has less effective positive charge than 2+. Consequently, such under-bonded  $O^{2-}$  ions may ionize by the reverse of step 4, eq'n (2), which is driven to the left. One way in which this may happen is by reaction with surface-adsorbed oxygen molecules in reactions such as:



leading variously to species such as  $O^-$  and  $O_2^-$  ions. Although we have no direct evidence for superoxide formation in the present rutile samples, it has been estimated that  $O_2^-$  and  $O^-$  ions are stable at the surfaces and bulk interior of binary oxides  $MeO^{26}$ . In addition, evidence for superoxide formation and  $p$ -type conductivity was found in Ca-doped  $BaTiO_3$  that had been re-oxidised after high temperature synthesis.<sup>27,28</sup> In that case, the concentration of superoxide ions was controlled by the oxygen vacancy concentration in the host lattice whereas here, we consider the possibility that they form more generally at sample surfaces.

In the  $p$ -type region, an excess of oxygen is required to trap the electrons that are released by ionization of under-bonded  $O^{2-}$  ions, eq'n (3). Consequently, the samples **should** show a resulting small oxygen excess,  $TiO_{2+\delta}$ , especially at the surfaces.

It was not possible to obtain an activation energy for conduction in the *p*-type region because first, the resistance was too high to measure at temperatures below ~450 °C, and second, at higher temperatures, conductivity Arrhenius plots are non-linear with an upward curvature (not shown), associated with the onset of oxygen loss. Hence, the carrier concentration was not constant during impedance measurements over the range 450-700 °C and the measured activation energy would contain both carrier creation and carrier mobility terms.

We propose a simple band structure model to account for the *p*-type behavior, as shown in Figure 7(B). The acceptor states are associated with adsorbed oxygen molecules on the sample surfaces; the holes are located at the top of the valence band on under-bonded, near-surface oxide ions. This model is essentially a surface-based model requiring, as a first step, the reversible adsorption/desorption of oxygen molecules on/from the sample surface. Since the binding energies of adsorbed oxygen molecules are not high, this is a low temperature model that is unlikely to lead to an equilibrium distribution of defects throughout the sample bulk and differs from the creation of immobile Ti vacancies that may be generated during prolonged oxidation at high temperatures.<sup>30</sup>

## 4. Conclusions

There is already an extensive literature on oxygen non-stoichiometry in rutile<sup>12-15</sup> and comprehensive fundamental studies on defect equilibria in TiO<sub>2</sub>.<sup>16-21</sup> Here, we focus on the main defect characteristics that dominate the structural and electrical properties and report two new observations associated with oxygen stoichiometry variation and its structural consequences in rutile.

First, in the early stages of oxygen loss, obtained by quenching samples from temperatures between 700 and 1000°C, chemical expansion occurs, shown by an

increase in lattice parameters, similar in nature to that seen in other oxides such as CeO<sub>2</sub> and ZrO<sub>2</sub>.<sup>9</sup> This expansion is attributed to weakening and lengthening of the Ti-O bonds on reduction.

Second, in the later stages of oxygen loss, on quenching samples from higher temperature and especially, for samples heated in an atmosphere of low pO<sub>2</sub>, the opposite effect of chemical contraction occurs and is attributed to partial structural collapse associated with elimination of oxygen vacancies and CS plane formation. As far as we are aware, this is the first reported example of a chemical contraction effect. On further oxygen loss, a homologous series of more heavily-reduced Magneli phases of formula Ti<sub>n</sub>O<sub>2n-1</sub> is expected, although was not seen here.

The occurrence of *n*-type semi-conductivity and associated darkening is well-established in oxygen-deficient rutile. Oxygen loss commences in air at temperatures as low as ~650 °C and can be detected because the conductivity is extremely sensitive to small levels of oxygen deficiency. At slightly lower temperatures, rutile is likely to be oxygen stoichiometric, but at 450 to 500 °C, the onset of *p*-type semi-conductivity is observed. It is attributed to reaction of underbonded O<sup>2-</sup> ions at sample surfaces with gas phase O<sub>2</sub> molecules and therefore, the TiO<sub>2</sub> has a slight oxygen excess. The holes reside on oxygen, ideally as O<sup>-</sup> ions.

The occurrence of *p*-type conductivity is commonly observed in [undoped](#) ceramic oxides and is widely attributed in the literature to the presence of unavoidable impurities such as Fe. It is, of course, very difficult to avoid small amounts of such impurities but similar *p*-type behavior to that seen here has been reported in a range of acceptor-doped titanate ceramics prepared from high purity chemicals. Under-bonded oxide ions, such as those associated with either acceptor dopants or located at sample surfaces, are likely to have reduced ionization potentials. This is because the free O<sup>2-</sup> ion in the gas phase is spontaneously unstable and is stabilized in crystal lattices only because of the extra lattice energy associated

with divalent anions compared to monovalent anions. It therefore appears likely that holes based on oxygen may be a general feature of *p*-type conductivity in many ceramic materials. [The under-bonded oxide ions that become the location of holes may be associated with either the presence of acceptor dopants or they could be oxide ions located at sample surfaces and interfaces.](#)

We also report the additional possibility of partial oxide ion conduction, especially in the *p-n* crossover region where electronic conductivity is minimised and oxygen vacancies are created. [A similar suggestion has been made previously.](#)<sup>30</sup>

## References

1. Yang HY, Zhu SK, Pan N. Studying the mechanisms of titanium dioxide as ultraviolet-blocking additive for films and fabrics by an improved scheme. *J Appl Polym Sci.* 2004;92:3201-3210.
2. Bach U, Lupo D, Moser JE, et al. Solid-state dye-sensitized mesoporous TiO<sub>2</sub> solar cells with high photon-to-electron conversion efficiencies. *Nature.* 1998;395:583-585.
3. Nakata K, Fujishima A. TiO<sub>2</sub> photocatalysis: design and applications. *J Photochem Photobiol C.* 2012;13:169-189.
4. Wu J, McCreery RL. Solid-state electrochemistry in molecule / TiO<sub>2</sub> molecular heterojunctions as the basis of the TiO<sub>2</sub> memristor. *J Electrochem Soc.* 2009;156:29-37.
5. Liu Y, West AR. Semiconductor-insulator transition in undoped rutile TiO<sub>2</sub> ceramics. *J Am Ceram Soc.* 2013;96:218-222.
6. Yang CY, Wang Z, Lin TQ, et al. Core-shell nanostructured black rutile titania as excellent catalyst for hydrogen production enhanced by sulfur doping. *J Am Chem Soc.* 2013;135:17831-17838.



7. Stoneham AM, Durham PJ. The ordering of crystallographic shear planes: theory of regular arrays. *J Phys Chem Solids*. 1973;34:2127-2135.
8. Blanchin MG, Faisant P, Picard C, et al. Transmission electron microscope observations of slightly reduced rutile. *Phys Stat Sol*. 1980;60:357-364.
9. Marrocchelli D, Bishop SR, Tuller HL, et al. Understanding chemical expansion in non-stoichiometric oxides: ceria and zirconia case studies. *Adv Funct Mater*. 2012;22:1958-1965.
10. Bishop SR. Chemical expansion of solid oxide fuel cell materials: a brief overview. *Acta Mech Sinica*. 2013;29:312-317.
11. Liu Y, West AR. Voltage-dependent resistance of undoped rutile TiO<sub>2</sub> ceramics. *Appl Phys Lett*. 2013;103:263508.
12. Lee DK, Jeon JI, Kim MH, et al. Oxygen non-stoichiometry ( $\delta$ ) of TiO<sub>2- $\delta$</sub> -revisited. *J Solid State Chem*. 2005;178:185-193.
13. Marucco JF, Gautron J, Lemasson P. Thermogravimetric and electrical study of non-stoichiometric titanium dioxide TiO<sub>2-x</sub>, between 800 and 1100 °C. *J Phys Chem Solids*. 1981;42:363-367.
14. Valentin CD, Pacchioni G. Reduced and n-type doped TiO<sub>2</sub>: nature of Ti<sup>3+</sup> species. *J Phys Chem C*. 2009;113:20543-20552.
15. Regonini D, Adamaki V, Bowen CR, et al. AC electrical properties of TiO<sub>2</sub> and Magnéli phases. *Solid State Ionics*. 2012;229:38-44.
16. Nowotny MK, Bak T and Nowotny J. Electrical properties and defect chemistry of TiO<sub>2</sub> single crystal. I Electrical conductivity. *J Phys Chem*. 2006; 110:16270-16282
17. Nowotny MK, Bak T and Nowotny J. II Thermoelectric power. *J Phys Chem*. 2006; 110:16283-16291
18. Nowotny MK, Bak T and Nowotny J. III Equilibration kinetics and chemical diffusion. *J Phys Chem*. 2006; 110:16292-16301
19. Nowotny MK, Bak T and Nowotny J. IV Prolonged oxidation kinetics and chemical diffusion. *J Phys Chem*. 2006; 110:16302-16308

20. Nowotny J, Alim MA, Bak T, Idris MA, Ionescu M, Prince K, Sahdan MZ, Sopian K, Teridi MAM and Sigmund W. Defect chemistry and defect engineering of TiO<sub>2</sub>-based semiconductors for solar energy conversion. *Chem Soc Rev.* 2015; 44: 8424-8442
21. Balachandran U and Eror NG. Electrical conductivity in non-stoichiometric titanium dioxide at elevated temperatures. *J Mater Sci.*1988; 23: 2676-2682
22. Guo M, Maso N, Liu Y and West AR. Electrical properties and oxygen stoichiometry of Ba<sub>1-x</sub>Sr<sub>x</sub>TiO<sub>3</sub> ceramics. *Inorg Chem.* 2018; 57: 64-71
23. Diebold W. The surface science of titanium dioxide. *Surf Sci Rep.* 2003; 48: 53-229
24. Wendt W *et al.* The role of interstitial sites in the Ti 3d defect state in the band gap of titania. *Science.* 2008; 320 1755-1759
25. Setvin M *et al.* Reaction of O<sub>2</sub> with subsurface oxygen vacancies on TiO<sub>2</sub> anatase (101). *Science.* 2013; 341: 988-991
26. Bielanski A, Haber J. Oxygen in catalysis on transition metal oxides. *Catal Rev Sci Eng.* 1979; 19:1-41.
27. Ren PR, Masó N, West AR. Hole conductivity in oxygen-excess BaTi<sub>1-x</sub>Ca<sub>x</sub>O<sub>3-x+δ</sub>. *Phys Chem Chem Phys.* 2013;15:20943-20950.
28. Ren PR, Masó N, Liu Y, et al. Mixed oxide ion and proton conduction and p-type semi-conduction in BaTi<sub>0.98</sub>Ca<sub>0.02</sub>O<sub>2.98</sub> ceramics. *J Mater Chem C.* 2013;1:2426-2432.
29. Masó N, West AR. Electrical properties of Ca-doped BiFeO<sub>3</sub> ceramics: from p-type semi-conduction to oxide-ion conduction. *Chem Mater.* 2012;24:2127-2132.
30. Nowotny MK, Sheppard LR, Bak T, Nowotny J. Defect Chemistry of Titanium Dioxide. Application of Defect Engineering in Processing of TiO<sub>2</sub>-Based Photocatalysts. *J Phys Chem.C* 2008; 5275-5300.

## List of figures

- 1** Lattice parameters and cell volume against quench temperature; samples were quenched after annealing in either air or N<sub>2</sub>; data for a slow-cooled sample are also shown
- 2** Z\* plots of TiO<sub>2</sub> at 700 °C (A) in N<sub>2</sub>, air and O<sub>2</sub>; (B) C' data in N<sub>2</sub>, air and O<sub>2</sub>
- 3** Effect of atmosphere on the impedance of TiO<sub>2</sub> at 500 °C
- 4** Effect of atmosphere on the impedance of TiO<sub>2</sub> at 600 °C and 550 °C
- 5** Schematic dependence of conductivity on atmosphere
- 6** Arrhenius plot of bulk conductivity data after different heat treatments: SC, slow-cooled in air; Q, quenched into liquid N<sub>2</sub>.<sup>5</sup>
- 7** (A) Occupied discrete [inter-gap](#) states and *n*-type conductivity associated with oxygen loss and (B) *p*-type conductivity associated with oxygen adsorption

## Supplementary Figure

**FIGURE S1** XRD data for quenched and slow-cooled TiO<sub>2</sub>

**TABLE S1** Chemical analysis of raw powder